RESEARCH ARTICLE

Key Points:
- Hourly averages are required to show a statistically significant mass density response during high geomagnetic activity
- The response of mass density for high geomagnetic activity intervals is strongest when $F_{10.7}$ is elevated
- There is no solar wind variation signature associated with large mass density events

Correspondence to:
R. S. Weigel,
rweigel@gmu.edu

Solar wind, $F_{10.7}$, and geomagnetic activity relationship to the equatorial plasma mass density at geosynchronous orbit

V. Veibell[1], R. S. Weigel[1], and R. E. Denton[2]

[1]Physics & Astronomy, George Mason University, Fairfax, Virginia, USA, [2]Physics & Astronomy, Dartmouth College, Hanover, New Hampshire, USA

Abstract We consider two types of events, identified by decreases in *Dst* below a threshold value and increases in the equatorial mass density at geosynchronous altitudes, ρ_{eq}, above a threshold value using the Takahashi et al. (2010) data set. From the *Dst* events and 1 day averages, we find that there is a statistically weak and small-amplitude difference between ρ_{eq} on the day of the event and the days before and after. When hourly averages are considered, a significant peak is found to occur 6 h after event onset, and the primary factor that determines the postonset peak amplitude in ρ_{eq} is elevated $F_{10.7}$. In addition, for hourly averages, ρ_{eq} following the onset of a *Dst* event depends on the north-south component of the interplanetary magnetic field, B_z, after the time of onset, with higher average B_z 4 h after the event onset corresponding to larger ρ_{eq} values 7–11 h after onset. From the ρ_{eq} events, we find a weak dependence on B_z after the onset of an event, with higher average B_z 4 h after the event onset corresponding to larger ρ_{eq} values 24–36 h after onset.

1. Introduction

The dependence of the plasmapause location on geomagnetic activity was observed as early as *Carpenter* [1966], and there are well-validated models of the plasmapause location as a function of L, MLT, and geomagnetic activity [*Lemaire*, 1998; *Moldwin et al.*, 2002; *O'Brien and Moldwin*, 2003]. Models also exist for the plasmasphere density [*Gallagher et al.*, 1988; *Lemaire*, 1998] with similar parameterization.

The dependence of the plasma density outside of the nominal plasmapause location on geomagnetic and solar wind conditions has not been extensively studied until the past decade [*Takahashi et al.*, 2006, 2010; *Denton et al.*, 2016]. Earlier works that considered profiles of ion density found a significant dependence of the plasmapause location on geomagnetic activity [*Chappell et al.*, 1970; *Maynard and Grebowsky*, 1977; *Carpenter and Anderson*, 1992], but the relationship between geomagnetic activity and density outside of the plasmapause was not explicitly considered.

Takahashi et al. [2006] estimated magnetospheric mass density using measurements from the CRRES satellite during a 73 day period in 1991 when CRRES was in an elliptical, near-equatorial orbit and primarily beyond the nominal plasmapause. They found that the local average ion mass, *M*, had some correlation with geomagnetic activity, with more negative hourly *Dst* values corresponding to higher *M* and longer 1.5 and 3 day averages of *Kp* corresponding to higher *M* (3 h averages of *Kp* had little visual correlation with *M*). The mass density estimates were obtained from CRRES observations in the MLT range of [12:00, 18:00] with most observations at *L* between 5 and 7 R_E.

Denton et al. [2006] found a weak relationship between *Dst* and *Kp* and the field line distribution of plasma mass density, ρ, using observations of the first three toroidal Alfvén harmonic frequencies for *L* in the range of 6–8 R_E. A more pronounced peak in the distribution along a field line near the equator was found for lower *Dst* and larger *Kp*, but the equatorial value of ρ was found to be similar for *Dst* bins of [−142, −31] and [−31, 37] nT and *Kp* bins of [1.5,3.4] and [3.4, 5.9].

Takahashi et al. [2010] developed a mass density data set using measurements from the Space Environment Monitor instruments on the Geostationary Operational Environmental Satellites (GOES) satellites from 1980 to 1992, with most measurements in the range of $L = 6.8 \pm 0.2\ R_E$. The mass density was estimated using the Alfvén wave velocity relationship, $V_A = B/\sqrt{\mu_0 \rho}$, a storm time magnetic field model, and a numerical solution
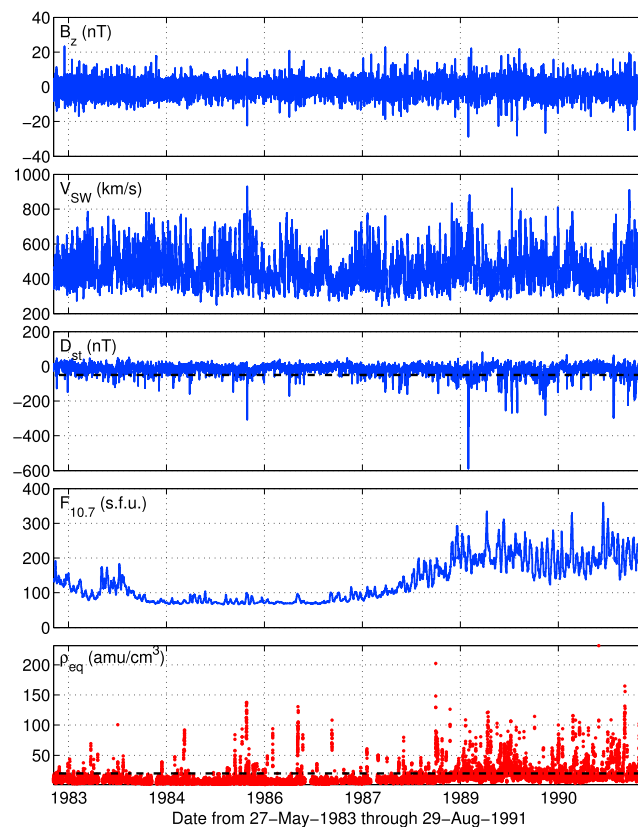
Figure 1. Overview of data used in this article. (first to fourth panels) Parameters from *Kondrashov et al.* [2014] and (fifth panel) ρ_{eq} based on GOES 6 measurements from *Denton* [2007] after interpolation and averaging described in the text. Dashed horizontal lines in the *Dst* and ρ_{eq} panels indicate sample event cutoff thresholds of *Dst* = −50 nT and ρ_{eq} = 20 amu/cm³ considered in section 3.

to a wave equation with an ionospheric boundary and the assumption of a zero resistance ionosphere. The equatorial mass density, ρ_{eq}, was derived from the estimated mass density using a power law dependence on the geocentric distance to the field line of the observation, R, $\rho = \rho_{eq}(LR_E/R)^{1/2}$. They found a high correlation (~0.94) between 27 day averages of $F_{10.7}$ and 27 day medians of ρ_{eq}.

Takahashi et al. [2010] noted that downward drops in the *Dst* index coincided with significant changes in ρ_{eq} for L near 6.8 R_E. For five storms, two had ρ_{eq} increases after *Dst* minimum, two had ρ_{eq} increases before the minimum, and one showed little change in ρ_{eq}. A key result was that when daily averaged measurements were considered, the epoch average of *Dst* for storms with a minimum *Dst* < −50 nT showed an enhancement in ρ_{eq} the same day as minimum *Dst* in the epoch averages.

Yao et al. [2008] studied the relationship between *Dst* and the number density of low-energy O^+ in different regions (ring current and plasma sheet) using the TEAMS and ESA instruments on the low-altitude and high-inclination orbiting FAST satellite and found that the average N_{O^+} across the sampled L shells (2–14) had a strong correlation (0.88) with the minimum *Dst* of the storm. Although the correlation at geosynchronous distances was not calculated, the data presented for four events show that the enhancements in N_{O^+} tended to appear near *Dst* minimum (±2 h).

The above results indicate that (1) the mass density at geosynchronous distances is best correlated with $F_{10.7}$ and (2) there exists a much weaker statistical relationship between mass density and the geomagnetic activity indices *Kp* and *Dst*. In this work we consider the dependence of mass density estimates in the *Takahashi et al.* [2010] data set and attempt to identify and statistically characterize the relationship between geomagnetic activity with mass density at geosynchronous distances. In addition, we attempt to identify solar wind variables that may drive or be associated with the changes.
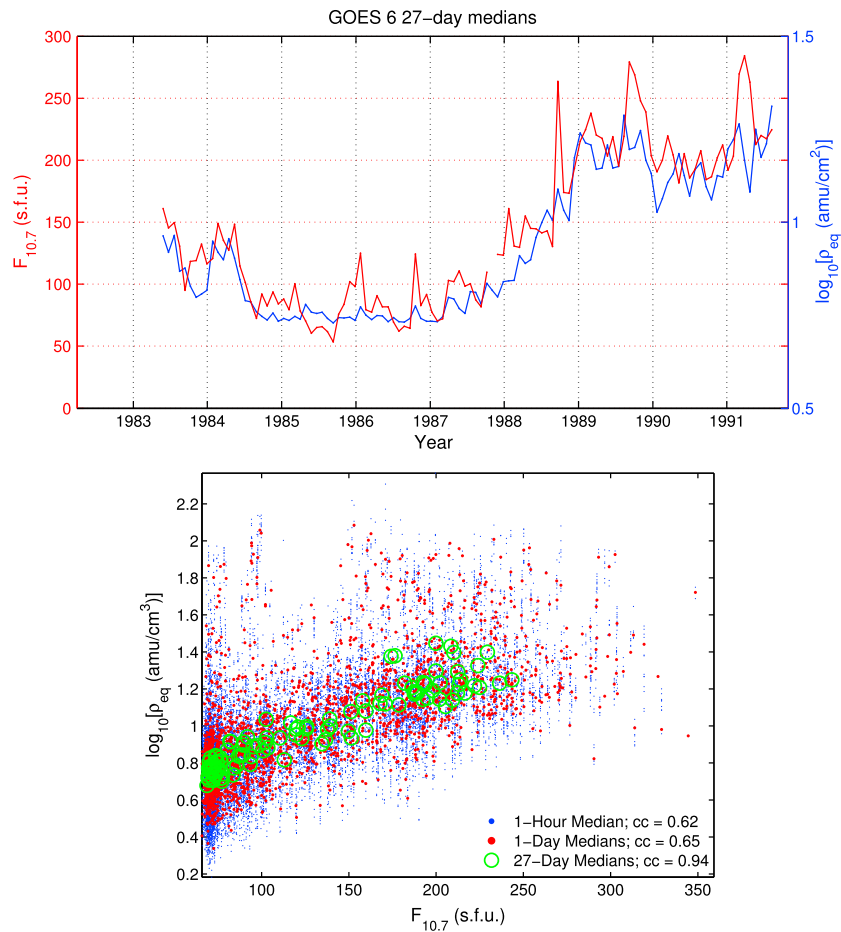
Figure 2. (top) The 27 day nonoverlapping medians of $F_{10.7}$ and $\log_{10}(\rho_{eq})$ from GOES 6. (bottom) Scatterplot of $\log_{10}(\rho_{eq})$ and $F_{10.7}$ using medians in nonoverlapping hour, day, and 27 day windows.

2. Data Preparation and Overview

The parameters ρ_{eq} and $F_{10.7}$ are from the data set of *Takahashi et al.* [2010], and data are available from 1980 to 1991 from GOES 2, 3, 5, 6, and 7. All other parameters used are from *Kondrashov et al.* [2014], which has coverage from 1972 to 2013 and are on a 1 h time grid. ρ_{eq} is the inferred equatorial mass density based on the third harmonic torodial frequency of magnetic field measurements as described in *Takahashi et al.* [2010]. The smallest cadence for ρ_{eq} values is 10 min. To compute an hourly median over the same interval for which the solar wind parameters were averaged, the median of all ρ_{eq} values in a given hour window was used. GOES 6 had the longest span (May 1983 to August 1991) of available data, and the primary results presented are for GOES 6, while measurements from other satellites were used for consistency checks. These data are shown in Figure 1.

Figure 2 (top) shows the long-term trends of $\log_{10}(\rho_{eq})$ from GOES 6 and $F_{10.7}$ computed using the median values in 27 day nonoverlapping windows. A scatterplot of these two lines is shown in Figure 2 (bottom) along with that for 1 day and 1 h medians. The linear correlation for GOES 6 using all measurements is found to be 0.94, which is the same value documented by *Takahashi et al.* [2010] who used combined measurements from all satellites in the time interval of 1980 through 1991 using the constraint $06:00 \leq MLT \leq 12:00$, $Kp_{3d} \geq 1.0$ and $Dst \geq -50$ nT. Our 27 day correlations for GOES 2, 5, and 7 are 0.81, 0.78, and 0.87, and the time range of coverage of measurements from these satellites is 1980-01-01/1983-05-16 — 1 January 1980/16 May 1983, 1983-01-01/1987-02-28 — 1 January 1983/28 February 1987, and 1983-05-27/1991-08-29 — 27 May 1983/29 August 1991, respectively.
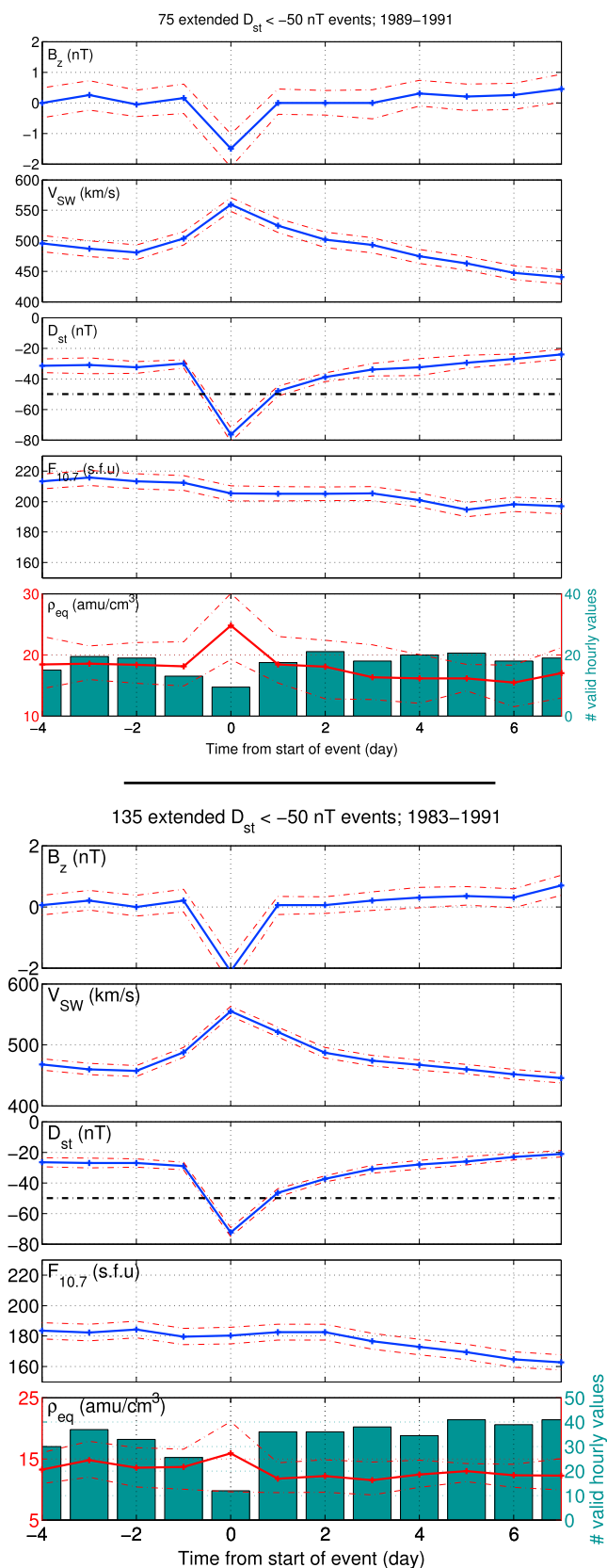
Figure 3. *Dst* events from GOES 6 using daily medians. (top) Events in the interval 1989–1991, compare to *Takahashi et al.* [2010, Figure 11]. (bottom) Events in the interval 1983–1991.

Table 1. Results of Test on of Medians of ρ_{eq} Shown in Figure 3 (Top) Between Days of Threshold Crossing Near (Day = 1 or −1) or on the Day of a *Dst* Event (Day = 0)

Days	Difference (amu/cm^3)	%
−1 0	−4.48	10.90% ≥ 0
−1 1	−1.46	34.30% ≥ 0
1 0	−3.02	21.50% ≥ 0

3. Results

Two types of events are considered. The first is a drop in the *Dst* index below the threshold value of −50 nT. These types of events are considered in order to determine if there is a well-defined ρ_{eq} dependence on geomagnetic activity as indicated by the *Dst* index. It is expected that the plasmasphere will exhibit two responses near the time of these threshold crossings. First is the movement of the plasmapause earthward [*Lemaire*, 1998], and the second is a possible change in density due to magnetospheric processes.

The second type of event is an increase in ρ_{eq} above a threshold of 20 amu/cm^3. It is expected that some of these increases will typically occur after a period of quiet geomagnetic activity. In this case, the plasmapause boundary may move outward past geosynchronous orbit, and the increase will be due to measurements being made inside the plasmapause. A second possible reason for the increase could be due to the same mechanism associated with increases that occur during enhanced geomagnetic activity.

3.1. *Dst* Events

Our first analysis uses GOES 6 data only from the time interval 1989–1991, which corresponds to the interval used in the epoch analysis of *Takahashi et al.* [2010]. In this interval, there were 75 *Dst* events where *Dst* remained below the −50 nT threshold for at least 12 h. Only events with an onset time when the spacecraft was located between 06:00 and 12:00 magnetic local time (MLT) were considered. The first hour of a local minimum in *Dst* following a threshold crossing defines the zero epoch time, and for each event, 4 · 24 h were considered before and 8 · 24 h after onset. For multiple detected threshold crossings within 24 h of each other, the first crossing was selected as the event onset because visual inspection showed the subsequent crossings to typically be from brief downward deviations during the recovery period of a geomagnetic storm. To compute the epoch averages on a daily time scale, the median value of all available measurements for all events centered on a window of ±12 h of the epoch zero hour was computed, and these averaging windows were shifted in increments of 24 h. Similar results are obtained if we first reduce each event time series to have a 1 day cadence by computing medians for each event in 1 day bins and then compute the medians across the averaged event time series on each epoch day.

The stack plot in Figure 3 (top) shows the epoch averages for the 75 events from 1989 to 1991 using data from GOES 6. The minimum *Dst* median is −75 nT. Consistent with *Takahashi et al.* [2010], *Dst* events correspond to elevated ρ_{eq} on the day of the event relative to the day before and after, although the magnitude of increase observed here is 4.5 amu/cm^3 instead of the increase of ~10 amu/cm^3 found in Figure 11 of *Takahashi et al.* [2010]. The vertical green bars in the ρ_{eq} plot show the number of ρ_{eq} values that were used to compute the medians and red error lines. The uncertainty is shown with error lines for each parameter that have a width that is twice the standard deviation of the values used in computing the median divided by the square root of the number of values. For the non-ρ_{eq} parameters, the number of measurements used in computing the medians is typically equal to the number of events, which is much larger than the number of ρ_{eq} values as all available measurements were used instead of restricting to only values where a ρ_{eq} value also existed.

In Figure 3 (bottom), it is shown that the trends seen in the analysis of 1989–1991 also hold for the entire span of measurements from GOES 6 (with coverage years of 1983–1991) — a small elevation on the day of the event relative to the day before and day after, with median averages after the day of the event being slightly lower than that before. A similar result is obtained for GOES 7 (1987–1991); the result is much less significant for GOES 5 (1983–1987) and is much more significant for GOES 2 (1981–1983). This trend has a relationship with the average value of $F_{10.7}$ during each respective coverage period, with the most significance found during the 1981–1983 time interval when $F_{10.7}$ was consistently elevated.
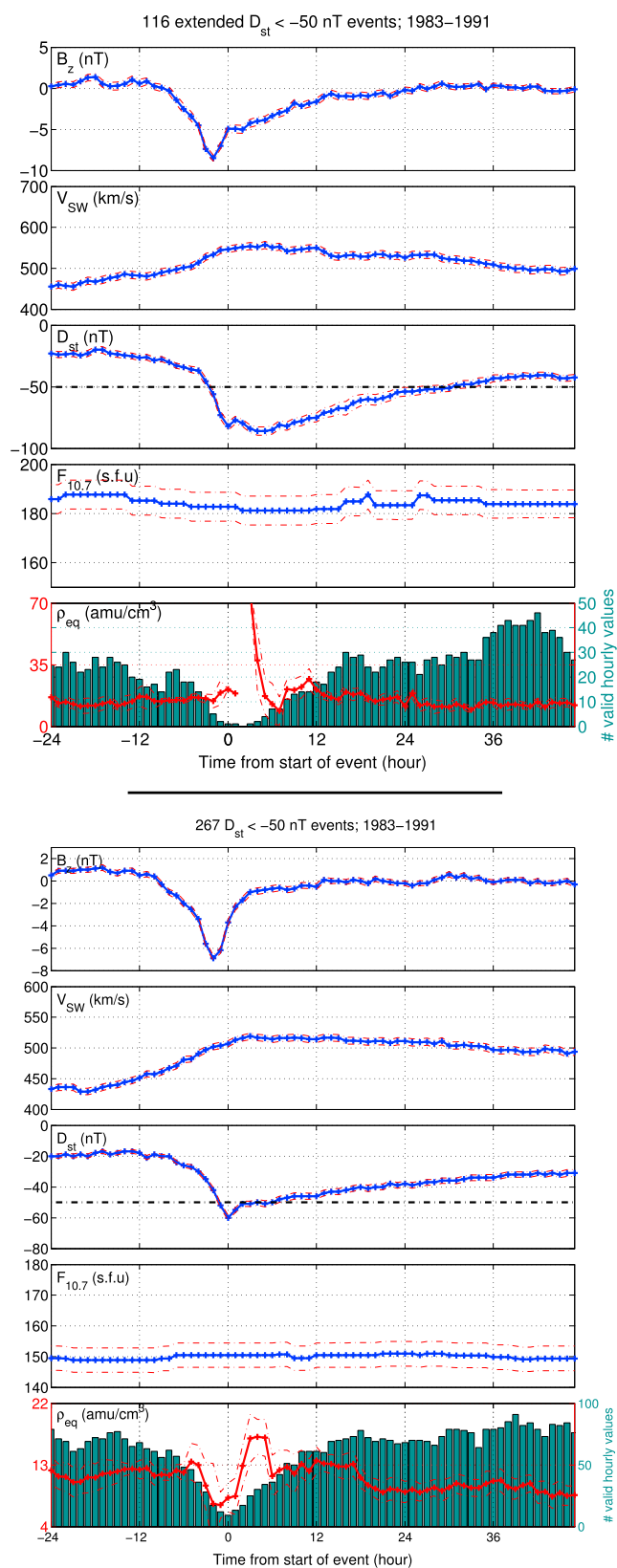
Figure 4. *Dst* events from GOES 6 using hourly medians. (top) Events with the constraint that *Dst* stayed below −50 nT for at least 12 h after crossing below −50 nT. (bottom) Same as Figure 4 (top) except without the 12 h constraint.
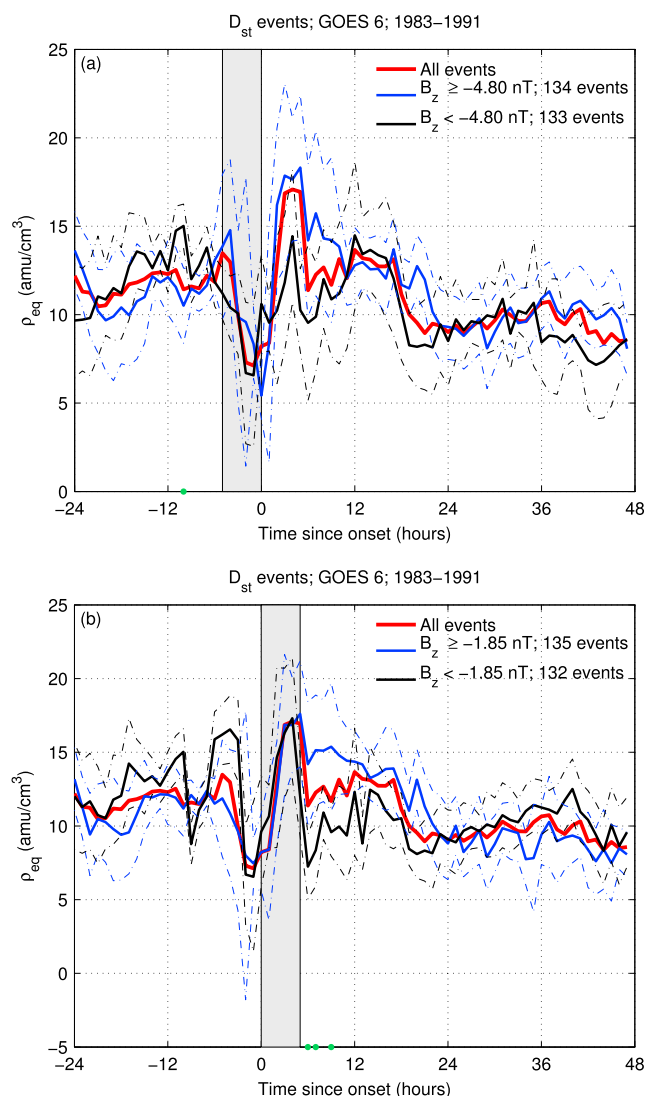
Figure 5. *Dst* events of Figure 4 (bottom) separated by the average *Dst* value (a) at onset and 4 h before and (b) at onset and 4 h after.

To determine if the magnitude of the density medians in Figure 3 (top) on epoch days −1, 0, and 1 are statistically different from each other, we used a two-population bootstrap test. A bootstrap sample of the medians for each epoch day was created by sampling all values (with replacement) used to compute the median on each epoch day. The observed difference between the medians is shown in Table 1 along with the fraction of observations in 1000 bootstrap differences with a different sign than that observed.

If a statistically significant difference in the medians between 2 days existed, the fraction of bootstrap samples with a different sign is expected to be much smaller (<5%). In terms of a hypothesis test, we cannot reject the null hypothesis that the medians are the same with a confidence higher than 100 minus the percentage value shown in the table; the highest confidence level of 86% is in the difference between days −1 and 0.

A similar hypothesis test run for Figure 3 (bottom) yields a maximum confidence level of ∼85%. For verification, the significance values were also tested using a Wilcoxon rank-sum test and were found to be similar.

These tests indicate that there is not a statistically significant difference in medians of daily averaged ρ_{eq} on the day before and day after a threshold crossing in *Dst*. In addition, the observed differences are on the order of only 20% of the value of ρ_{eq} on the onset day, which is similar to the magnitude of variation in the observations over the displayed epoch time interval.
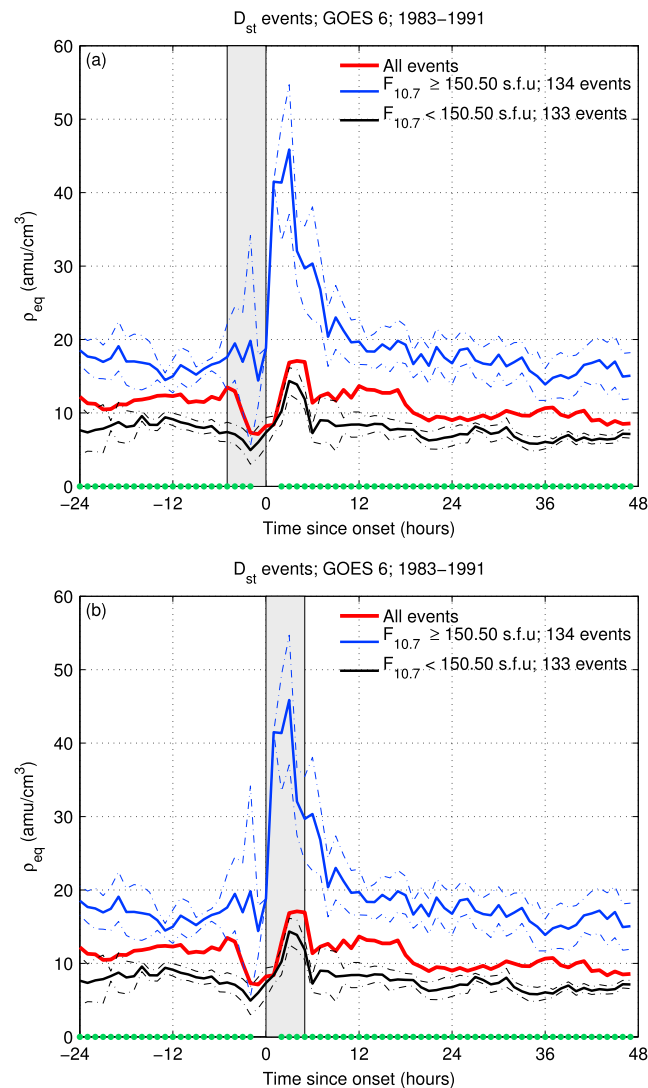
Figure 6. *Dst* events of Figure 4 (bottom) separated by the average $F_{10.7}$ value (a) at onset and 4 h before and (b) at onset and 4 h after.

We have also considered hourly averages of data for the events shown in Figure 3 (bottom), which are shown in Figure 4 (top). In the time period of elevated mass density within 6 h of the start of the event, there are only approximately four samples per hourly interval, and the peak value of ~70 amu/cm³ is associated with a single observation.

To increase the number of events, we have removed the constraint that the events must occur in the MLT range of 06:00–12:00 and the constraint that *Dst* remained below the threshold value for 12 h or longer. The result is shown in Figure 4 (bottom). The two variations from a baseline (one downward before onset and one upward after onset) were tested for significant deviation from two baselines, one 24–12 h before onset and one 16–48 h after onset. The probability of the downward variation coming from the same distribution as the data from the left baseline is 1.06%, whereas the probability of the right upward variation coming from the same distribution of the data for the right baseline is 0.17%. This significant result is also maintained for GOES 2, 5, and 7. This indicates that there are statistically significant variations in ρ_{eq} within 6 h of onset when hourly averages are considered. The significance of the upward variation result is consistent with previous observations of large mass density increases in the plasma trough region during large geomagnetic storms [*Yao et al.*, 2008; *Takahashi et al.*, 2010].
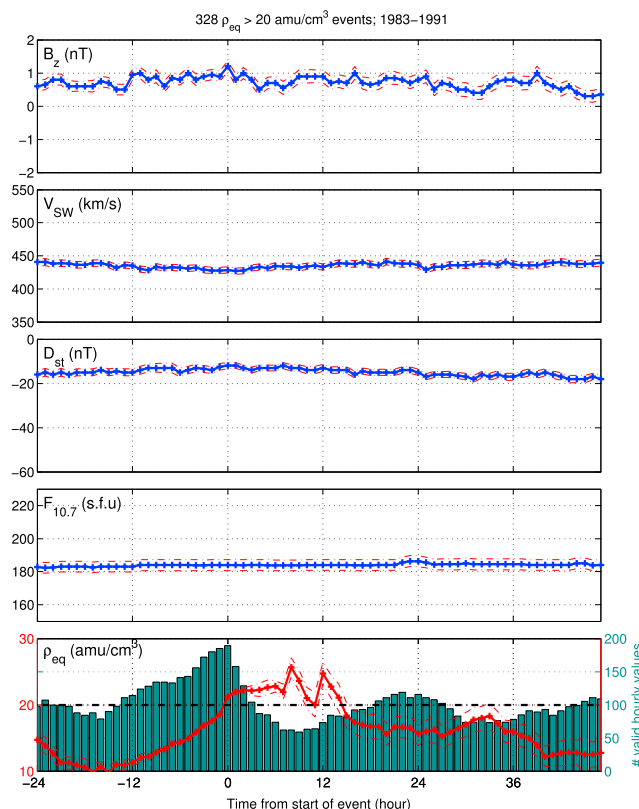
Figure 7. $\rho_{eq} > 20$ amu/cm^3 events from GOES 6 using hourly medians.

To determine if there is an interplanetary magnetic field B_z dependence, the epoch curves in Figure 4 (bottom) for ρ_{eq} and B_z were separated into two parts based on the median value of B_z within a window. One window covered the 4 h before onset and onset and the other covered onset and the following 4 h; the result is shown in Figure 5. Any statistically significant difference at a 95% confidence level between the two parts is indicated by a green dot on the horizontal axis using a Wilcoxon rank-sum test. For the case where the separation is made according to the value of B_z after onset, there is a visible and significant separation between the curves from 7 to 11 h after onset, with more negative B_z values corresponding to lower values of ρ_{eq}.

The process for creating Figure 5 was repeated except using the sort variable $F_{10.7}$ instead of B_z, and the result is shown in Figure 6. The difference between the epoch curves is statistically significant at all times, as expected due to the high correlation between ρ_{eq} and $F_{10.7}$, but elevated $F_{10.7}$ is associated with a peak in the ρ_{eq} curve approximately 5 h after onset. The values contributing to the peak were compared to a baseline of all values 16–48 h after onset via a Wilcoxon rank-sum test and were found to have significantly different medians at the 99% confidence level. This indicates the possibility that there must be a high preexisting baseline level of ρ_{eq} in order for an increase in ρ_{eq} to be observed for a *Dst* event. This result is also consistent with the analysis of Figure 3 when repeated using measurements from GOES satellites taken during different parts of the solar cycle; the significance of the differences between the days around onset was largest when the measurements were taken during time intervals when $F_{10.7}$ was consistently elevated.

3.2. ρ_{eq} Events

An alternative type of event can be defined that corresponds to large increases in ρ_{eq}. Figure 7 shows the epoch time series for events in which an increase of ρ_{eq} above 20 amu/cm^3 defines the start of the event. In finding ρ_{eq} events, missing values were replaced with linearly interpolated values. These events are associated with on-average positive B_z and small values of *Dst* with little variability. Approximately 12 h after onset, ρ_{eq} slowly decays over 36 h to near preonset levels.

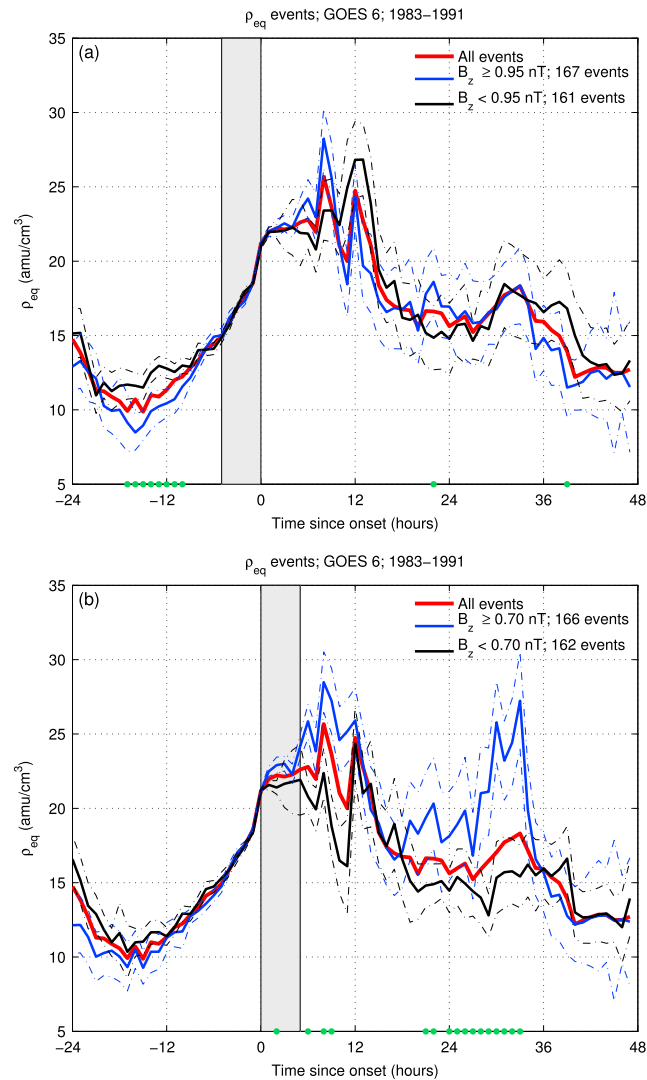**Figure 8.** ρ_{eq} events of Figure 7 separated by the average B_z value (a) at onset and 4 h before and (b) at onset and 4 h after.

Figure 7 can be compared with Figure 9 of *Denton et al.* [2016], which shows daily averages of ρ_{eq} from this data set after the onset of quiet Kp intervals. The growth shown here (using the ρ_m threshold criteria with no constraint on Kp) is approximately linear and lasts ∼12–18 h, whereas the 10 Kp events (elevated Kp followed by 2 days with $Kp \leq 1^+$) considered by *Denton et al.* [2016] showed growth that lasted for at least 48 h.

Figure 8 shows the events of Figure 7 when separated by B_z in the same manner as Figure 5. The largest difference occurs when the separation is performed after onset, with more positive B_z leading to a larger peak in ρ_{eq} than more negative B_z. The rate of change of ρ_{eq} also appears to be insensitive to the time windows used to determine the separation (before or after onset).

Figure 9 shows how the epoch average curve of ρ_{eq} in Figure 7 depends on $F_{10.7}$. Statistically significant differences occur independent of whether the separating factor is the average of $F_{10.7}$ before or after onset, as expected because the cadence of $F_{10.7}$ is 1 day, and its time scale of variation is longer than that of ρ_{eq}. Events with high $F_{10.7}$ are associated with higher ρ_{eq} before and after event onset but have similar peak values. As was the case for B_z, there is an approximately 12 h time span of linear growth of ρ_{eq} near the time of onset but because the initial starting ρ_{eq} is higher for high $F_{10.7}$, the associated growth rate is lower, consistent with *Denton et al.* [2016].
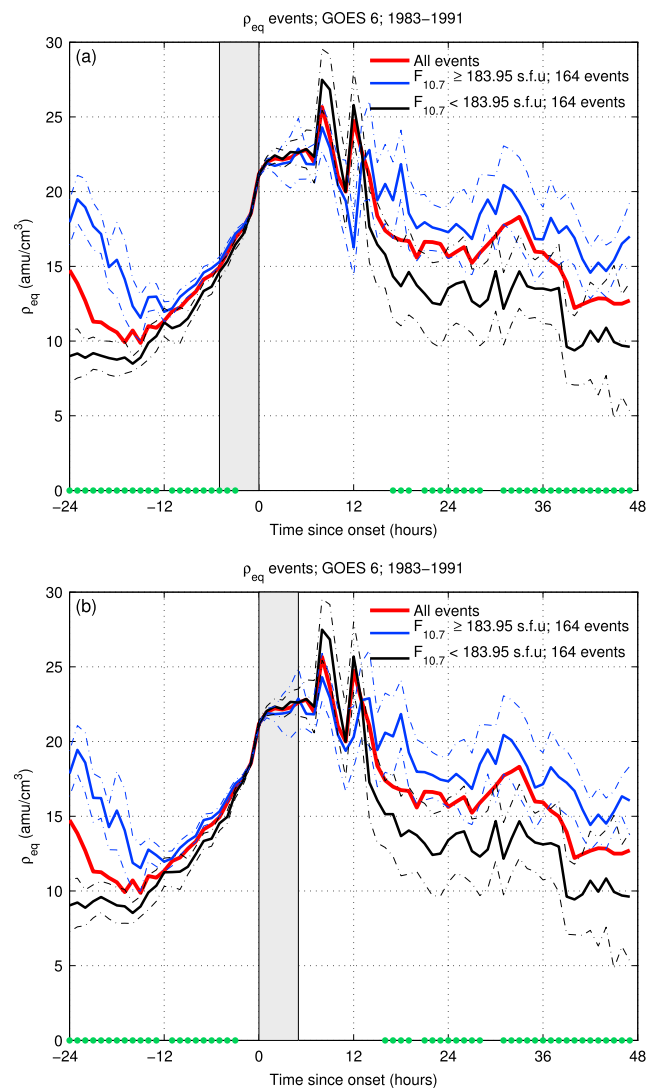
Figure 9. ρ_{eq} events of Figure 7 separated by the average $F_{10.7}$ value (a) at onset and 4 h before and (b) at onset and 4 h after.

3.3. Summary and Conclusions

In recent years, various works have considered the influence of solar wind control and the geomagnetic activity relationship to the equatorial plasma mass density at geosynchronous orbit, generally using event studies and linear correlations [*Takahashi et al.*, 2006; *Denton et al.*, 2006; *Yao et al.*, 2008; *Takahashi et al.*, 2010; *Denton et al.*, 2011, 2016]. The event studies show a possible relationship between ρ_{eq} and solar wind and geomagnetic activity indicators such as *Kp* and *Dst*, while correlation studies have generally found a very weak relationship.

This work presents an analysis of two types of events intended to provide insight into the relationship between ρ_{eq}, solar wind, and geomagnetic parameters by considering both large geomagnetic events and large ρ_{eq} events. The two types of events were considered in order to account for a difficulty with the identification of the cause in ρ_{eq} enhancements, which can occur for two reasons: (1) an extended period of positive B_z, which leads to low geomagnetic activity, plasmasphere refilling, and a possible expansion of the plasmasphere to geosynchronous altitudes and (2) strong negative B_z, which (a) leads to the inward motion of the higher density plasmasphere and leaves geosynchronous altitudes in the lower density plasma trough just outside of the plasmapause and (b) causes possible magnetospheric processes to enhance the mass density at geosynchronous altitudes.

On average, around the time of large geomagnetic events, there is a statistically weak enhancement of daily averaged ρ_{eq} measurements. For hourly averages, ρ_{eq} shows enhancements over a 6 h postonset window that contains too few events for a statistical analysis. When the constraint of extended geomagnetic events (greater than 12 h below a threshold value) and the spacecraft MLT for observation of ρ_{eq} (06:00 – 12:00) is removed to allow for more events, statistically significant variations are found, with a peak occurring approximately 6 h after the event onset. For the hourly averaged measurements, ρ_{eq} averages within 7 – 11 h after the onset time was lower when the average of B_z 4 h after the onset time was more positive. This result highlights the complexity of the response of ρ_{eq} to solar wind driving. Negative values of B_z are generally needed for a large geomagnetic event to occur, and we have shown an association between large geomagnetic events and increases in ρ_{eq} within 6 h of the event onset, but after the onset of the event, more positive values of B_z are associated with larger ρ_{eq} values.

It was shown that a key factor in determining if large ρ_{eq} enhancements will be observed is elevated $F_{10.7}$. When geomagnetic events were separated according to if they occurred when $F_{10.7}$ was low or high, larger enhancements in ρ_{eq} above a baseline value were only observed under high $F_{10.7}$ conditions. *Denton et al.* [2016] showed that the ratio of O^+/H^+ changes greatly with solar cycle, with larger amounts of O^+ occurring during solar maximum (when $F_{10.7}$ is elevated). The dependence of the mass density response on $F_{10.7}$ suggests that the process responsible for enhancing ρ_{eq} during geomagnetic storms may have a strong sensitivity to the O^+/H^+ ratio.

For ρ_{eq} events, more positive B_z after onset corresponded to higher values of subsequent ρ_{eq}, which indicates that a substantial portion of the events may be due to the apparent mass refilling mechanism described by *Denton et al.* [2016]. In order to separate this mechanism from an enhancement due to magnetospheric activity using this type of analysis, additional information about the location of the plasmapause may be required.

References

Carpenter, D. L. (1966), Whistler studies of the plasmapause in the magnetosphere: 1. Temporal variations in the position of the knee and some evidence on plasma motions near the knee, *J. Geophys. Res.*, *71*, 693–709.

Carpenter, D. L., and R. R. Anderson (1992), An ISEE/whistler model of equatorial electron density in the magnetosphere, *J. Geophys. Res.*, *97*, 1097–1108.

Chappell, C. R., K. K. Harris, and G. W. Sharp (1970), A study of the influence of magnetic activity on the location of the plasmapause as measured by OGO 5, *J. Geophys. Res.*, *75*, 50–56.

Denton, R. (2007), *Database of Input Parameters for Tsyganenko Magnetic Field Models*.

Denton, R. E., K. Takahashi, I. A. Galkin, P. A. Nsumei, X. Huang, B. W. Reinisch, R. R. Anderson, M. K. Sleeper, and W. J. Hughes (2006), Distribution of density along magnetospheric field lines, *J. Geophys. Res.*, *111*, A04213, doi:10.1029/2005JA011414.

Denton, R. E., M. F. Thomsen, K. Takahashi, R. R. Anderson, and H. J. Singer (2011), Solar cycle dependence of bulk ion composition at geosynchronous orbit, *J. Geophys. Res.*, *116*, A03212, doi:10.1029/2010JA016027.

Denton, R. E., K. Takahashi, J. Amoh, and H. J. Singer (2016), Mass density at geostationary orbit and apparent mass refilling, *J. Geophys. Res. Space Physics*, *121*, 2962–2975, doi:10.1002/2015JA022167.

Gallagher, D. L., P. D. Craven, and R. H. Comfort (1988), An empirical model of the Earth's plasmasphere, *Adv. Space Res.*, *8*, 15–21.

Kondrashov, D., R. Denton, Y. Y. Shprits, and H. J. Singer (2014), Reconstruction of gaps in the past history of solar wind parameters, *Geophys. Res. Lett.*, *41*, 2702–2707, doi:10.1002/2014GL059741.

Lemaire, J. (1998), *The Earth's Plasmasphere*, Cambridge Univ. Press, New York.

Maynard, N. C., and J. M. Grebowsky (1977), The plasmapause revisited, *J. Geophys. Res.*, *82*, 1591–1600.

Moldwin, M. B., L. Downward, H. K. Rassoul, R. Amin, and R. R. Anderson (2002), A new model of the location of the plasmapause: CRRES results, *J. of Geophys. Res.*, *107*(A11), 1339, doi:10.1029/2001JA009211.

O'Brien, T. P., and M. B. Moldwin (2003), Empirical plasmapause models from magnetic indices, *Geophys. Res. Lett.*, *30*(4), 1152, doi:10.1029/2002GL016007.

Takahashi, K., R. E. Denton, R. R. Anderson, and W. J. Hughes (2006), Mass density inferred from toroidal wave frequencies and its comparison to electron density, *J. Geophys. Res.*, *111*, A01201, doi:10.1029/2005JA011286.

Takahashi, K., R. E. Denton, and H. J. Singer (2010), Solar cycle variation of geosynchronous plasma mass density derived from the frequency of standing Alfvén waves, *J. Geophys. Res.*, *115*, A07207, doi:10.1029/2009JA015243.

Yao, Y., K. Seki, Y. Miyoshi, J. P. McFadden, E. J. Lund, and C. W. Carlson (2008), Effect of solar wind variation on low-energy O^+ populations in the magnetosphere during geomagnetic storms: FAST observations, *J. Geophys. Res.*, *113*, A04220, doi:10.1029/2007JA012681.